ISBN: 978-3-95450-247-9 ISSN: 2673-5490 doi: 10.18429/JACoW-IPAC2024-TUPC03

# MULTI-BUNCH BEAM DYNAMICS STUDIES FOR THE C$^3$ MAIN LINAC

W. H. Tan*, G. White, Z. Li, E. A. Nanni
SLAC National Accelerator Laboratory, Menlo Park, CA, USA
D. Kim, H. Xu, E. Simakov
Los Alamos National Laboratory, Los Alamos, NM, USA



*Abstract*

The Cool Copper Collider (C$^3$) is a novel accelerator concept for a linear collider utilizing a cryogenically-cooled copper linear accelerator (linac) with a distributed coupling architecture. The C$^3$ main linac is designed to accelerate electron/positron from 10 GeV to 125 GeV while preserving the beam emittance. Here we present the analysis of the multi-bunch beam dynamics for the C$^3$ main linac. We show the beam dynamics simulation results of the C$^3$ main linac to identify the frequency bands that cause emittance growth and the amount of frequency detuning required to suppress it. Results presented will be used to guide the future design of the accelerating structure.

## INTRODUCTION

C$^3$ is an advanced normal-conducting radio-frequency (NCRF) linear accelerator utilizing a distributed coupling architecture to realize a $e^+e^-$ collider for the study of Higgs boson at 250 GeV with relatively low cost [1–3]. The C$^3$ main linac is designed to accelerate electron or positron beams from 10 GeV to 125 GeV, which translates to the center-of-mass (COM) energy of 250 GeV, with a planned upgrade to reach COM energy of 550 GeV using higher gradient on the same linac structure. In order to reach the target luminosity for Higgs production, emittance needs to be preserved throughout the whole collider. The source of emittance degradation in the main linac includes short and long range wakefield effects of the accelerating structure, alignment and vibration errors of the linac components. Hence, iterations of beam dynamics studies are required to assess the performance of the main linac and revise the design, such as design studies done by other collider proposals [4–8].

The beam requirements for C$^3$ are largely determined by the beam energy and luminosity necessary for precision studies of the Higgs boson at $e^+e^-$ collisions. For 250 GeV COM energy, Higgs boson is produced through the $e^+e^- \to ZH$ process, in which Higgs bosons are produced in association with a $Z$ boson. Through this process, Higgs bosons can be identified independent of their decay products by reconstructing the invariant mass of the recoil against an identified $Z$ boson, and exploiting the well-defined four-momentum of the initial $e^+e^-$ state. Thus, properties of the Higgs boson, such as its mass, branching fractions and couplings to fermions and gauge bosons can be measured in a model-independent way to percent or sub-percent precision [9]. A target luminosity of $1.3 \times 10^{34}$ cm$^{-2}$ s$^{-1}$ has been set for C$^3$ at 250 GeV. In order to achieve this luminosity, assuming a bunch charge of 1 nC and a bunch length of 100 μm, normalized horizontal (vertical) emittances at the IP of 900 (20) nm and beta functions at the IP of 12 (0.12) mm have been proposed for the nominal C$^3$ parameter set, as summarized in Table 1.

Table 1: Design Parameters for the Main Linac of C$^3$

| Parameter | Value | Unit |
|---|---|---|
| Initial beam energy | 10 | GeV |
| Final beam energy | 125 | GeV |
| Bunch charge | 1 | nC |
| Bunch length | 100 | μm |
| Initial emittance in x,y | 775, 10 | nm |
| Final emittance in x,y | 900, 20 | nm |
| Initial rms beam size in x,y | 20,1.6 | μm |
| Initial energy spread | 1.5 | % |
| Final energy spread | 0.34 | % |
| Number of bunches | 133 | - |
| Bunch spacing | 5.25 | ns |

## LINAC DESIGN

The main linac is an array of FODO cells, where each FODO cell is assembled as a cryomodule that includes four 0.15 m alternating focusing and defocusing quadrupoles and eight 1 m, 40 cells C-band (5.712 GHz) accelerating structures, as shown in Fig. 1. Lattice parameters of FODO cells must be adjusted along the linac so that the beta function grows with the square root of the beam energy along the linac [4, 10, 11]. The relation between the phase advance of the first FODO cell, $\mu_1$, and the phase advance of the n$^{\text{th}}$ FODO cell, $\mu_n$, is given by

$$\tan\frac{\mu_n}{2} = \tan\frac{\mu_1}{2}\left(\frac{\gamma_1}{\gamma_n}\right)^{0.5}, \quad (1)$$

where $\gamma_1$ and $\gamma_n$ are beam energies at the first and n-th FODO cell. The geometric strength, $K_{1,n}$ and length $L_n$ of the quadrupole of the n-th FODO cell is calculated as

$$K_{1,n}L_n = K_{1,1}L_1\left(\frac{\sin\mu_n/2}{\sin\mu_1/2}\right). \quad (2)$$

## MULTI-BUNCH BEAM DYNAMICS

### *Long-Range Wakefields*

Long-range wakefields are known to contribute to the emittance growth in multi-bunch beam dynamics, in par-

* whtan@slac.stanford.edu

ISBN: 978-3-95450-247-9 ISSN: 2673-5490 doi: 10.18429/JACoW-IPAC2024-TUPC03

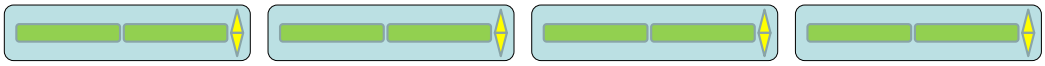

Figure 1: The C$^3$ main linac consists of an array of FODO cells, each FODO cell has four quadrupoles (yellow rhombuses) paired with eight C-band accelerating structures (green rectangles).

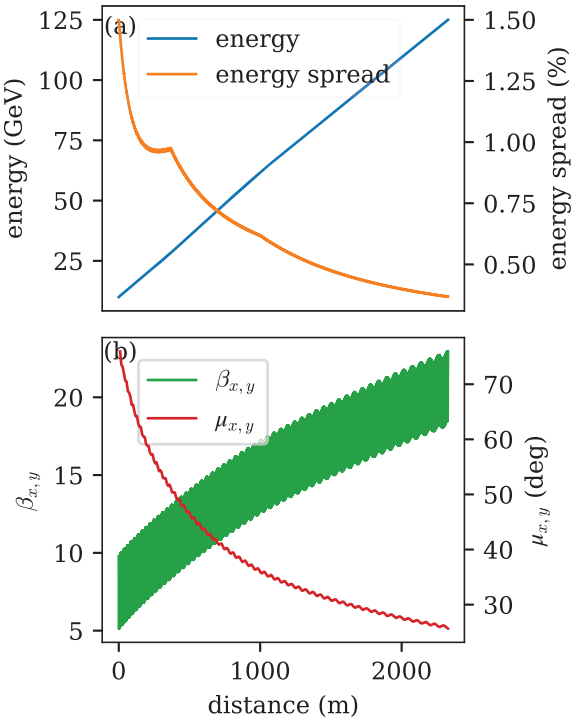


Figure 2: The evolution of the beam energy is shown in (a), whereas the evolution of the Twiss parameters $\beta_x$, $\beta_y$ and phase advances $\mu_x$, $\mu_y$ are shown in (b).

ticular due to the transverse higher-order-modes (HOMs). Damping and detuning of long-range wakefields were the subject of extensive design studies for collider designs such as NLC and CLIC [4, 6]. The general approach to addressing the effects of long-range wakefields includes the use of both damping (decreasing the Q-factors of HOMs), and detuning or controlling the frequency and spectrum of HOMs. In our current design, we employed waveguide slots with Nickel-Chromium (Nichrome) absorbers to provide damping to the HOMs [12]. Figure 3 shows the Q-value ($Q_n$) times kick factor ($\kappa_n$), where subscript $n$ denotes the n-th mode.

### *Simulation Setup*

The setup for multi-bunch simulation studies is detailed in Table 1. In order to focus on investigating the effect of HOMs, we neglected short-range wakefields in our simulations. We generated random initial offsets in the y-direction for all 133 bunches with the rms offset of 0.3 µm. A total of 100 simulations with random initial offsets were performed to investigate the effect of HOMs.

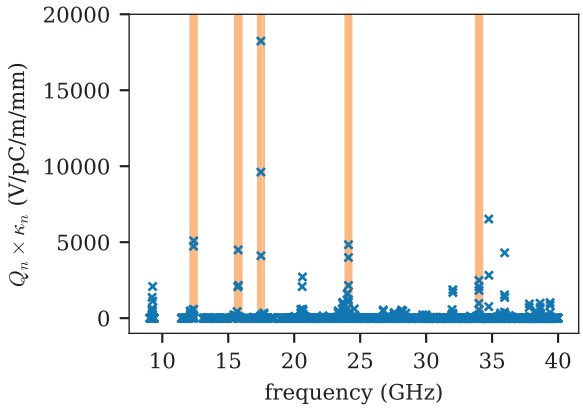


Figure 3: Plot of Q times kick factor versus frequency for the long-range wakefields, up to 40 GHz. Frequency bands that cause emittance growth are highlighted in orange.

### *Gaussian Detuning of HOMs*

We surmised that the distribution of HOMs can be described by a Gaussian function, where HOMs with very high kick factor are due to the sum of modes of all 40 cells in the accelerating structure. We performed Gaussian detuning by specifying the frequency width of each mode, and redistributed HOMs to effectively lowering the kick factor. Physically, frequency detuning can be realized by adjusting the shapes of cells in accelerating structure to change frequencies of HOMs in different cells within a certain frequency rms width.

## RESULTS AND DISCUSSIONS

Figure 4 shows the final emittance of all 133 bunches from tracking simulation with long-range HOMs. A total of 100 Monte Carlo simulations with random initial offsets for all 133 bunches were performed. The blue shaded region represents the upper and lower limit of the beams' emittance from these 100 simulations, whereas the solid blue line represent the average. The orange dotted line represent the case with the largest emittance growth. The electron bunches' centroids exhibit the oscillating pattern. These patterns correspond to frequency bands that are causing emittance growth, as highlighted in orange in Fig. 3.

We ran multi-bunch simulations with different values of frequency RMS width for detuning to investigate the required frequency RMS width to suppress the emittance growth. Figure 5 shows a plot of the largest emittance of the bunch train versus the RMS frequency width used for detuning. The inset shows that the decrease of emittance reaches a minimum after the RMS frequency width reaches 80 MHz. Con-

ISBN: 978-3-95450-247-9 ISSN: 2673-5490 doi: 10.18429/JACoW-IPAC2024-TUPC03



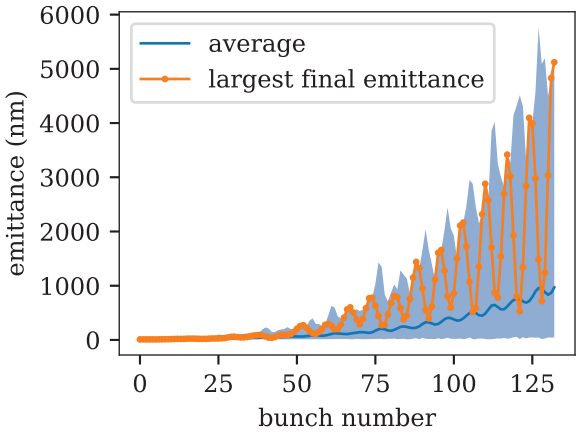


Figure 4: Final emittance of all 133 bunches from Elegant tracking simulation with long-range wakefields. A total of 100 Monte Carlo simulations with random initial offsets for all 133 bunches were performed. The blue shaded region represents the upper and lower limit of the beams' emittance from these 100 simulations, whereas the solid blue line represent the average. The orange dotted line represent the case with the largest emittance growth. The electron bunches' centroids exhibit the oscillating pattern.

sequently, the final emittance of all bunches with 80 MHz detuning width is shown in Fig. 6.

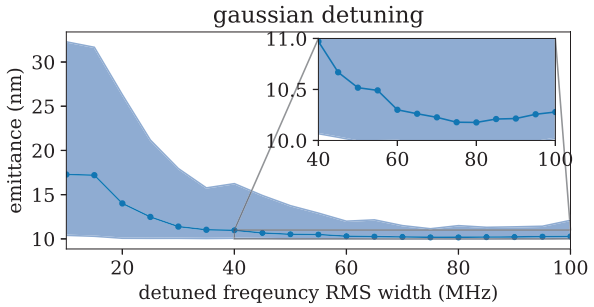


Figure 5: This is the plot of the largest emittance of the bunch train versus the RMS frequency width used for detuning. The inset shows that emittance growth can be suppressed down to 10.3 nm with 80 MHz detuning width.

## CONCLUSION

In summary, this paper presents the design of the $C^3$ main linac and the results of multi-bunch beam dynamics. Multiple bunch simulation results identify important frequency bands that contribute to the emittance growth. In addition, we also found the required detuning frequency width to suppress the emittance growth.

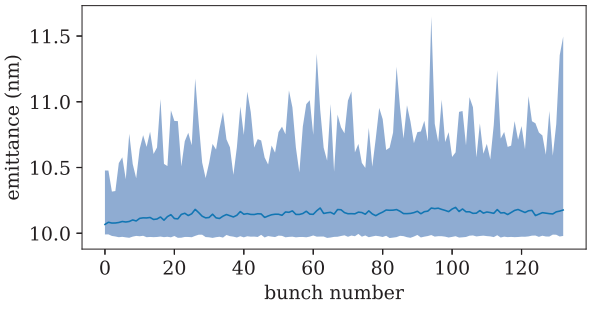


Figure 6: Final emittance of all 133 bunches with 80 MHz detuning width. The emittance growth is suppressed.

## ACKNOWLEDGMENTS

W.H.T. thanks M. Borland, R. Soliday and A.J. Dick (ANL) for discussions on using Elegant. This work was supported by the U.S. Department of Energy Contract No. DE-AC02-76SF00515 with SLAC National Accelerator Laboratory, and Contract No. DE-AC52-06NA25396 with Los Alamos National Laboratory. Simulation works used resources of the National Energy Research Scientific Computing (NERSC) Center, U.S. Department of Energy Office of Science User Facility located at Lawrence Berkeley National Laboratory, operated under Contract No. DE-AC02-05CH11231.

## REFERENCES

[1] K. L. Bane *et al.*, *An advanced ncrf linac concept for a high energy $e^+e^-$ linear collider*, 2019.

[2] S. Tantawi, M. Nasr, Z. Li, C. Limborg, and P. Borchard, "Design and demonstration of a distributed-coupling linear accelerator structure," *Phys. Rev. Accel. Beams*, vol. 23, no. 9, p. 092 001, 2020.

[3] C. Vernieri *et al.*, "Strategy for understanding the higgs physics: The cool copper collider," *JINST*, vol. 18, 2023. doi:10.48550/arXiv.2203.07646

[4] T. N. D. Group, "Zeroth-Order Design Report for the Next Linear Collider," SLAC National Accelerator Laboratory, SLAC Report SLAC-474, 1996. https://www.slac.stanford.edu/accel/nlc/zdr/

[5] S. Stapnes, "The Compact Linear Collider," *Nature Reviews Physics*, vol. 1, no. 4, pp. 235–237, 2019. doi:10.1038/s42254-019-0051-5

[6] O. Brunner *et al.*, *The CLIC project*, 2022. doi:10.48550/arxiv.org/abs/2203.09186

[7] C. Adolphsen *et al.*, *The International Linear Collider Technical Design Report - Volume 3.I: Accelerator R&D in the Technical Design Phase*, 2013. doi:10.48550/arXiv.1306.6353

[8] C. Adolphsen *et al.*, *The International Linear Collider Technical Design Report - Volume 3.II: Accelerator Baseline Design*, 2013. doi:10.48550/arxiv.org/abs/1306.6328

[9] A. Aryshev *et al.*, "The International Linear Collider: Report to Snowmass 2021," 2022.

ISBN: 978-3-95450-247-9 ISSN: 2673-5490 doi: 10.18429/JACoW-IPAC2024-TUPC03

[10] T. O. Raubenheimer, "The generation and acceleration of low emittance flat beams for future linear colliders," SLAC National Accelerator Laboratory, SLAC Report SLAC-387, 1991. doi:10.2172/5816546

[11] V. M. Tsakanov, "Autophasing and lattice scaling in high energy linear accelerators," *Phys. Rev. ST Accel. Beams*, vol. 1, p. 041 001, 4 1998. doi:10.1103/PhysRevSTAB.1.041001

[12] D. Kim, Z. Li, and E. Simakov, "Study of HOM couplers for the c-band accelerating structure," in *Proc. IPAC'23*, Venice, Italy, 2023, pp. 2053–2056. doi:10.18429/JACoW-IPAC2023-TUPL136